

# Fractals and log-periodic corrections applied to masses and energy levels of several nuclei

B. Tatischeff<sup>1,2</sup>

<sup>1</sup>Univ Paris-Sud, IPNO, UMR-8608, Orsay, F-91405

<sup>2</sup>CNRS/IN2P3, Orsay, F-91405\*

A contribution is presented to the application of fractal properties and log-periodic corrections to the masses of several nuclei (isotopes or isotones), and to the energy levels of some nuclei. The fractal parameters  $\alpha$  and  $\lambda$  are not randomly distributed, but take a small number of values, common also with the values extracted previously from fractal distributions of quark, lepton, and hadronic masses. Several masses of still unobserved nuclei are tentatively predicted.

## I. INTRODUCTION

The powerful concept of fractals [1], has been applied to the study of a large number of different fields (see for example [2]). However, up to now, to my knowledge, only one attempt was done to look whether the fractal properties were appropriate to describe, at least partly, the many properties of nuclear physics. The hadronic, lepton, and gauge boson masses, have been already discussed within a fractal scaling model of a chain system of quantum harmonic oscillators [3]. It was shown there, that "Scaling is a fundamental property of any natural oscillation process". The author interpreted the elementary particle masses as being proton resonances. He uses a different model but also on the logarithmic scale. This approach is different from our approach.

Several particle physics ratios, and strength ratios, were discussed within a "Higgs free symmetry breaking from critical behavior near dimension four" model [4].

Before starting the present study, several steps were elaborated:

- first, several relations between nearly all elementary particle masses were found [5]. The masses of quarks, gauge bosons, and leptons were reproduced, starting for each species with the lowest mass, using nucleon and pion masses, and fine structure constant value;

- then, it was shown that the fractal properties agree to describe the fundamental force coupling constants, the atomic energies, and the elementary particle masses [6]. This agreement was obtained using the discrete-scale invariance model (DSI) [7] [8];

- finally the fractal properties were applied with success to the hadronic masses [9]. It was found that the parameters used to fit the mass ratios between all adjacent masses of a given species, display the same distribution for all hadronic species.

The very large number of properties concerning nuclear physics, asks for an attempt to rely these properties to each others, as much as possible, in order to reduce the number of free values. These properties are the nuclear masses, their energy level masses, the total and partial widths for all excited levels, the quantum numbers .... Below, we will discuss some of these properties within the fractal description, precisely to look for eventual common descriptions.

### A. The fractal characteristic of hadronic masses

The fractal concept stipulates that the same physical laws apply for different scales of a given physics [10]. We summarize here briefly the concept of continuous and discrete scale invariances transcribing the developpements of D. Sornette [7] and L. Nottale [2]. The concept of *continuous* scale invariance is defined in the following way: an observable  $O(x)$ , depending on the variable  $x$ , is scale invariant under the arbitrary change  $x \rightarrow \lambda x$ , if there is a number  $\mu(\lambda)$  such that  $O(x) = \mu O(\lambda x)$ .  $\lambda$  is the fundamental scaling ratio. The solution of  $O(x)$  is the power law:

$$O(x) = Cx^\alpha \quad (1)$$

where  $\alpha = -\ln\mu/\ln\lambda$ .

The relative value of the observable, at two different scales, depends only on  $\mu$ , the ratio of the two scales  $O(x)/O(\lambda x)$  and does not depend on  $x$ . We have therefore " a continuous translational invariance expressed on the logarithms of the variables". If the distribution of the logarithm of  $O(x)$  versus the logarithm of  $x$ , displays a straight line, we expect that a relation exists allowing the fit by the DSI model, and allowing the calculation of the masses, starting from the lowest mass.

---

\* tati@ipno.in2p3.fr

## B. The discrete scale invariance characteristic of hadronic masses

The *discrete* scale invariance (DSI), in opposition to the *continuous* scale invariance, is observed when the scale invariance is only observed for specific choices of  $\lambda$ . Its signature is the presence of power laws with complex exponents  $\alpha$  inducing log-periodic corrections to scaling [7]. In case of DSI, the  $\alpha$  exponent is

$$\alpha = -\ln\mu/\ln\lambda + i2n\pi/\ln\lambda \quad (2)$$

where  $n$  is an arbitrary integer. The *continuous* scale invariance is obtained for the special case  $n = 0$ , then  $\alpha$  becomes real.

The critical exponent "s" is defined by  $\mu = \lambda^s$ . Defining  $\Omega = 1/\ln\lambda$ , we obtain  $\alpha = -s + i2\pi\Omega$ .

The most general form of distributions following DSI was given by Sornette [7]. We apply it to the ratio of two hadronic adjacent masses of a given species, "f(r)", where "r" is the rank of the distribution. Following the most general form of the mass ratio distribution f(r):

$$f(r) = C (|r-r_c|)^s [1+a_1 \cos(2\pi \Omega \ln (|r-r_c|)+\Psi)] \quad (3)$$

where we have omitted the imaginary part of f(r).

C is a normalization constant.  $a_1$  measures the amplitude of the log-periodic correction to continuous scaling, and  $\Psi$  is a phase in the cosine. " $r_c$ " is the critical rank, which describes the transition from one phase to another. It is underdetermined, but widely larger than the experimental "r" values. This is the general situation of hadronic mass ratios. Such undetermination has very few consequences on all parameters, except on  $\Omega$ . When increasing " $r_c$ " from 30 to 40,  $\Omega$  increases approximately by a factor 1.36. Therefore " $r_c$ " was arbitrarily fixed to " $r_c$ " = 40 for all following studies, the same value as the one used in the application of fractals for the study of hadronic masses [9].

In summary, the signature of scale invariances is the existence of power laws. The exponent  $\alpha$  is real if we have continuous scale invariances and is complex in case of discrete scale invariances, and then gives rise to log-periodic corrections.

We first plot the log of the studied quantity, versus the log of its rank ( $\ln(R)$ ), defined as being the mass number from the lighter to the heavier studied mass. All masses are expressed in MeV.

Then we study the ratio of successive values fitted by equation (3).

## II. APPLICATION TO NUCLEI MASSES

In all following applications, when the fundamental nuclei masses are studied, they are introduced with increasing values of the variable Z (number of protons), N (number of neutrons), or the mass number A. The masses are

taken from the Atomic Mass Table [11]. They are very precise, therefore the errors, which are introduced in the computations, are not visible.

### A. Application to light nuclei with Z (then N) =1, 2, or 3

FIG. 1. Log-log distribution of light nuclei masses. Full triangles (green on line) show the distribution for Z = 1 nuclei, A increasing from 1 up to 7. Full circles (red on line) show the distribution for Z = 2 nuclei, A increasing from 3 up to 10. Full squares (blue on line) show the distribution for Z = 3 nuclei, A increasing from 3 up to 12, (see text).

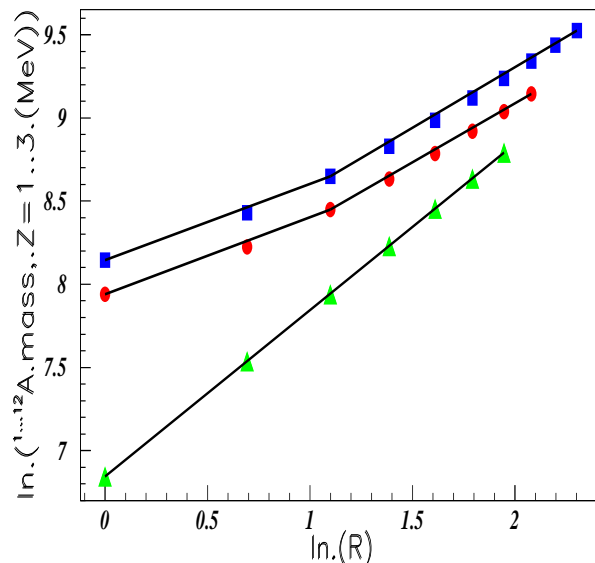


Figure 1 shows the log-log distribution of light nuclei masses [11] for constant number of protons ( $Z=1, 2, \text{ or } 3$ ) and increasing variable number of neutrons. Full triangles (green on line) show the distribution of  $Z = 1$  nuclei,  $A$  increasing from 1 ( $R = 1$ ) up to 7 ( $R = 7$ ). Full circles (red on line) show the distribution of  $Z = 2$  nuclei,  $A$  increasing from 3 ( $R = 1$ ) up to 10 ( $R = 8$ ). Full squares (blue on line) show the distribution of  $Z = 3$  nuclei,  $A$  increasing from 3 ( $R = 1$ ) up to 12 ( $R = 10$ ). These last data, full squares (blue on line), are shifted vertically by the quantity  $\log(\text{shift}(\text{MeV})) = 0.2$ , in order to separate these data from the  $Z = 2$  data. The distributions exhibit straight lines, which indicate fractal properties.

The nice alignments of the log-log distributions suggest to extrapolate them in order to predict the masses of the next nuclei. The resulting results are given in table 1, where all masses are in MeV. The third column indicates the last (heavier) known experimental mass, followed by the same mass calculated using the previous masses and the linearity of the log-log distributions. The relative precision between both is given in the next column, and finally the predicted mass of the still unobserved nucleus is given in the last column.

FIG. 2. Ratios of  $m_{n+1}/m_n$  masses of several light nuclei. Full triangles (green on line) show the distribution of  $Z = 1$  nuclei,  $A$  increasing from 1 up to 7. Full circles (red on line) show the distribution of  $Z = 2$  nuclei,  $A$  increasing from 3 up to 10. Full squares (blue on line) show the distribution of  $Z = 3$  nuclei,  $A$  increasing from 3 up to 12.

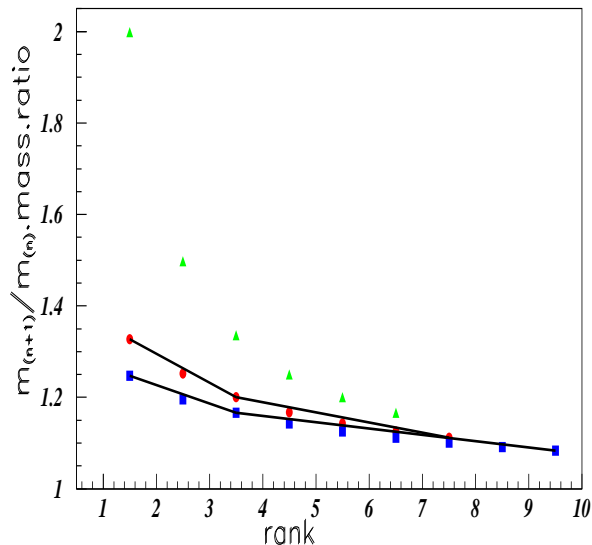


TABLE I. Experimental and "calculated" last observed masses with  $Z = 1, 2,$  and  $3$  nuclei corresponding to figure 1, then  $N = 1, 2,$  and  $3$  nuclei corresponding to figure 3. Each line ends by the next predicted, but (still) not observed mass. All masses are in MeV; the empty markers correspond to full markers of figure 1 and 3.

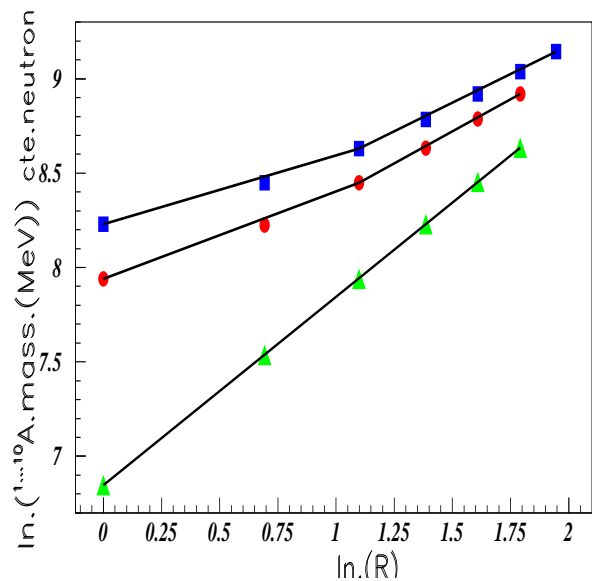
Fig.	Marker	last known		mass rel gap.	next predicted mass
		exper.	calcul		
1	$Z=1$ $\triangle$	6569.0	6568.63	$5.3 \cdot 10^{-5}$	${}^8\text{H}$ 7507.4
	2 $\circ$	9362.6	9244.4	1.3%	${}^{11}\text{He}$ 10179
	3 $\square$	11226.3	11095.2	1.2%	${}^{13}\text{Li}$ 12034
3	$N=1$ $\triangle$	5629.9	5631.4	$2.6 \cdot 10^{-4}$	${}^7\text{C}$ 6567.5
	2 $\circ$	7483.8	7385.4	1.3%	${}^9\text{N}$ 8312.3
	3 $\square$	9350.0	9204.4	1.6%	${}^{11}\text{O}$ 10136

The shape of the distributions, however, shown in figure 2, does not correspond to the oscillatory variation described by equation (3). The assumption could be advanced, that the low value of the maximum rank, due to the small number of such nuclei, could be responsible for the oscillation deficiency. This is probably not the case, since much lighter particles as quarks and leptons, display clear oscillations, in spite of a smaller number of elements, therefore a smaller maximum rank [6]. All data describing the  $m_{n+1}/m_n$  mass ratio, will be plotted at rank  $n+1/2$ .

Figure 3 shows the log-log distribution for light nuclei, constant number of neutrons "N", and variable number

of protons. Full triangles (green on line) show the distribution of  $N = 1$  nuclei,  $A$  increasing from 1 ( $R = 1$ ) up to 6 ( $R = 6$ ). Full circles (red on line) show the distribution of  $N = 2$  nuclei,  $A$  increasing from 3 ( $R = 1$ ) up to 8 ( $R = 6$ ). Full squares (blue on line) show the distribution of  $N = 3$  nuclei,  $A$  increasing from 4 ( $R = 1$ ) up to 10 ( $R = 7$ ). Here again straight lines indicate nice fractal properties. The shape of the three distributions, is like the one drawn for constant "Z" and shown in figure 1.

FIG. 3. Log-log distribution of light nuclei masses for constant number of neutrons "N". Full triangles (green on line) show the distribution of  $N = 1$  nuclei,  $A$  increasing from 1 up to 6. Full circles (red on line) show the distribution of  $N = 2$  nuclei,  $A$  increasing from 3 up to 8. Full squares (blue on line) show the distribution of  $N = 3$  nuclei,  $A$  increasing from 4 up to 10.

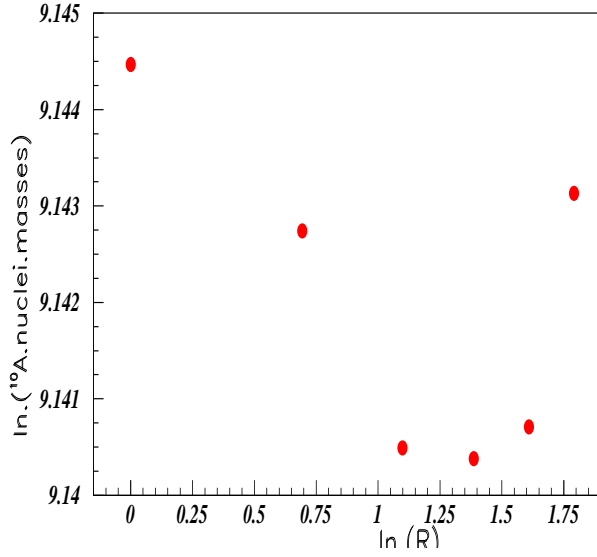


Here again, the nice alignments of the log-log distributions suggest to extrapolate them in order to predict the masses of next nuclei. The resulting results are given in table 1, where all masses are in MeV. The third column indicates the last experimental mass, followed by the corresponding calculated value. The calculated masses use again the linearity of the previous masses in the log-log distributions. The relative precision between both is given in the next column, and finally the predicted masses of the (still) unobserved nuclei are given in the last column.

## B. Application to $A = 10$ nuclei masses

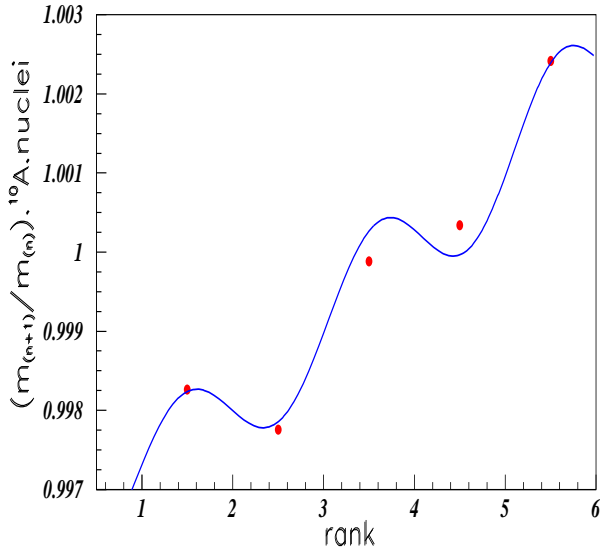
Only six masses of ten nucleons are reported in the PDG table [11]. Figure 4 shows that the data in the log-log plot are not aligned, therefore these data should not follow the fractal properties. We observe however that the  $m_{n+1}/m_n$  mass ratio of  $A = 10$  nuclei, versus the rank  $R$ , shown in figure 5, is rather well fitted by

FIG. 4. Log of  $A = 10$  nuclei masses versus the log of the rank "R".



equation (3). We conclude that the  $m_{n+1}/m_n$  mass ratio distribution, as described by equation (3), is more general, and could eventually be not restricted to data following fractal properties.

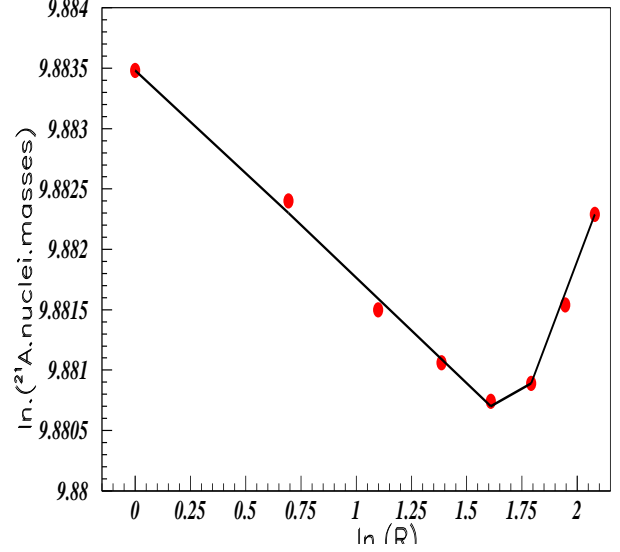
FIG. 5. Ratios of  $m_{n+1}/m_n$  masses versus the rank, for  $A = 10$  nuclei.



### C. Application to $A = 21$ nuclei masses

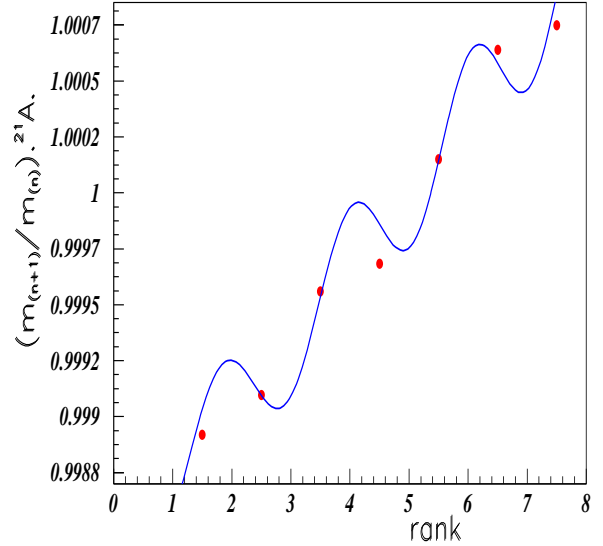
Figure 6 shows three log-log distributions for  $A = 21$  nuclei masses. In this figure, the first five masses, and the last three masses are aligned, which shows fractal properties. The corresponding  $m_{n+1}/m_n$  mass ratio versus the rank "R", is shown in figure 7. All seven data points

FIG. 6. Log of  $A = 21$  nuclei masses versus the log of the rank "R".



(except one (the fourth)), are well described by the fit. Although the amplitude of the oscillations, given by the parameter "a<sub>1</sub>" of equation (3), is poorly determined, the parameters "Ω" and "s", therefore the important parameters "α" and "λ" are well determined by the data.

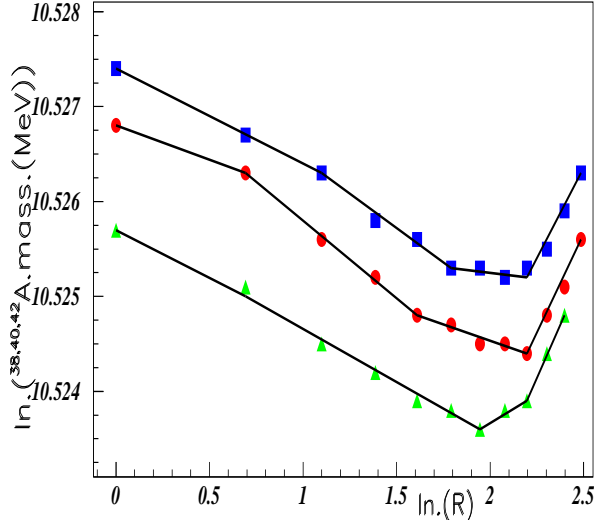
FIG. 7. Ratios of  $m_{n+1}/m_n$  masses, versus the rank "R", for  $A = 21$  nuclei.



### D. Application to nuclei with masses $A = 38, 40,$ and $42$

Figure 8 shows the log-log distribution of the  $A = 38, 40,$  and  $42$  nuclei masses (for increasing  $Z$  values), calculated with help of the mass excess table [11]. The  $Z$  values increase from 12 up to 22 for  $A = 38$  (rank=1 up to 11),

FIG. 8. Log-log distribution of three nuclei masses for increasing  $Z$  values. Full circles (red on line) show data for  $A=40$ . Full squares (blue on line) show results for  $A = 42$ , the log values of these data are shifted by  $-0.048$  in order to enter in the same figure. Full triangles (green on line) show results for  $A = 38$ ; the log values of these last data are shifted by  $+0.0505$  in order to enter in the same figure.



increase from 12 up to 23 for  $A = 40$  (rank = 1 up to 12), and increase from 13 up to 24 for  $A = 42$  (rank = 1 up to 12). Several alignments manifest the fractal properties of these data. In order to clarify the figure, the log values of these data for  $A = 38$  and  $42$  are shifted respectively by  $+0.0505$  and  $-0.048$  in the ordinate scale.

FIG. 9. Ratios of  $m_{n+1}/m_n$  masses versus the rank, for nuclei close to  $A = 40$ . Full circles (red on line) show data for  $A = 40$  and increasing  $Z$  values; full squares (blue on line) show results for  $A = 42$ ; full triangles (green on line) show results for  $A = 38$ .

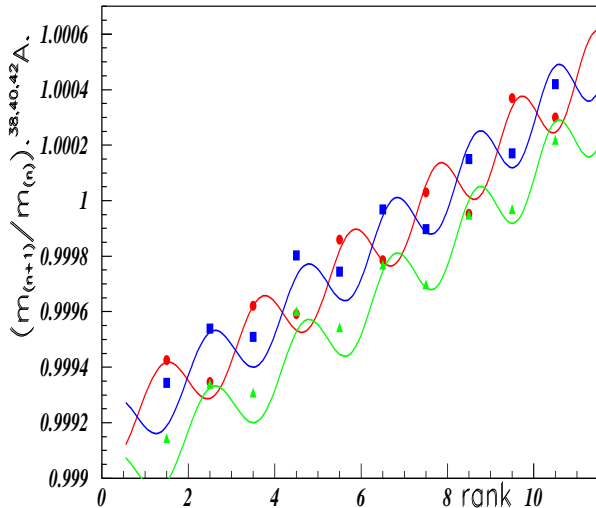


Figure 9 shows the  $m_{n+1}/m_n$  mass ratios, versus the rank, for nuclei in the  $A \approx 40$  nuclei and increasing  $Z$  values. Full circles (red on line) show data for  $A=40$ ; full squares (blue on line) show results for  $A = 42$ ; full triangles (green on line) show results for  $A = 38$ . The experimental ratio values of these last data, and the calculated curve, are renormalized by  $0.9998$  in order to be distinguished from  $A = 42$  nuclei data. The fit gives rise to clearly observed nice oscillations, which describe the data in the whole experimental range. All three curves are obtained using equation (3) and same parameters, except the phase  $\Psi$ , different for  $^{40}\text{A}$  and equal for  $^{38}\text{A}$  and  $^{42}\text{A}$ . As a matter of fact, the  $A = 38$  and  $42$  distributions are in phase in figure 9, when the  $A = 40$  distribution is in an opposite phase.

FIG. 10. Log of some nuclei masses around  $^{40}\text{Ca}$  versus the log of the rank "R". Insert (a) shows the distribution for calcium isotopes (full circles, red on line), the distribution of sulfur isotopes (full squares, blue on line), and the distribution of  $N = 20$  isotones (full triangles, green on line), slightly shifted (see text); insert (b) shows the distribution for  $A = 40$  nuclei.

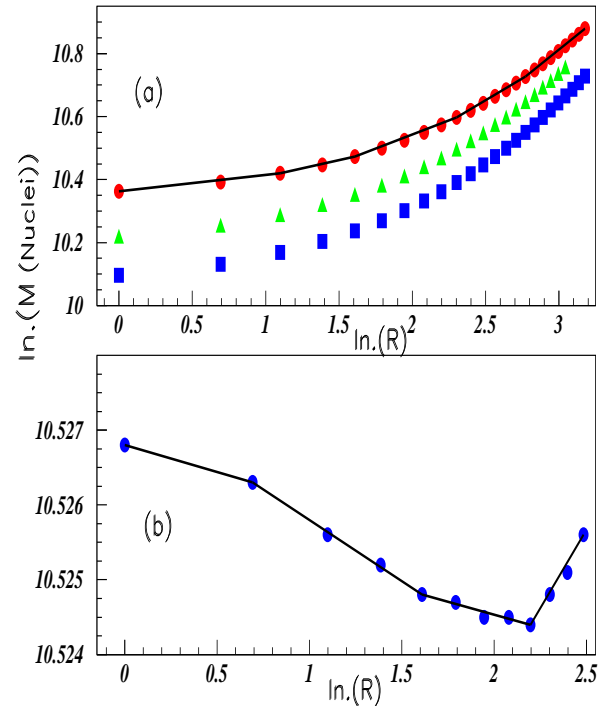


Figure 10 shows several log-log distributions for constant  $Z$  nuclei around  $^{40}\text{Ca}$ . Figure 10(a) shows the distribution for calcium isotopes (full circles, red on line), the distribution of sulfur isotopes (full squares, blue on line), and the distribution of  $N = 20$  isotones (full triangles, green on line). These last data are shifted by  $+0.05$  in order to separate them from the sulfur data. Figure 10(b) shows the distribution for  $A = 40$  nuclei, already shown in figure 8 where the variation displays several straight lines for the distribution corresponding

to the mass variation for  $A = 40$  nuclei. The fractal property of  $A = 40$  nuclei is more effective, than it was for calcium and sulfur isotopes, and  $N = 20$  isotones; it is however less effective than it was for light nuclei.

The linearity at the end of the distributions shown in figure 8, allows us to tentatively extrapolate the masses and predict the masses of still unobserved nuclei. Table II gives the last experimental observed masses of the  $A = 38, 40$ , and  $42$  nuclei, compared to the "calculated" masses. The calculated masses use the linearity of the previous masses in the log-log distribution. The relative errors between both lie between  $1.10^{-4}$  and  $2.10^{-4}$ . The last column shows the predicted mass of the next, still unobserved nuclei.

TABLE II. Experimental and "calculated" last observed masses for  $^{38,40,42}A$  nuclei corresponding to figure 8, followed by the next predicted, but still not observed, mass. All masses are in MeV. The empty markers here, correspond to the full markers in the figures.

	last	exprim.	mass	next mass
Marker	exper.	calcul	rel gap.	predicted
$A=38$	$\triangle$	35394.0	35397.6	$1.0 \cdot 10^{-4}$ $^{38}V$ 35405
40	$\circ$	37257.9	37249.7	$2.1 \cdot 10^{-4}$ $^{40}Cr$ 37268
42	$\square$	39115.8	39108.7	$1.8 \cdot 10^{-4}$ $^{42}Mg$ 39128

### E. Application to masses of $A = 99$ and $100$ nuclei

FIG. 11. Log of  $A = 100$  (full circles, red on line) and  $A = 99$  nuclei masses (full squares, blue on line) versus the log of the rank "R".

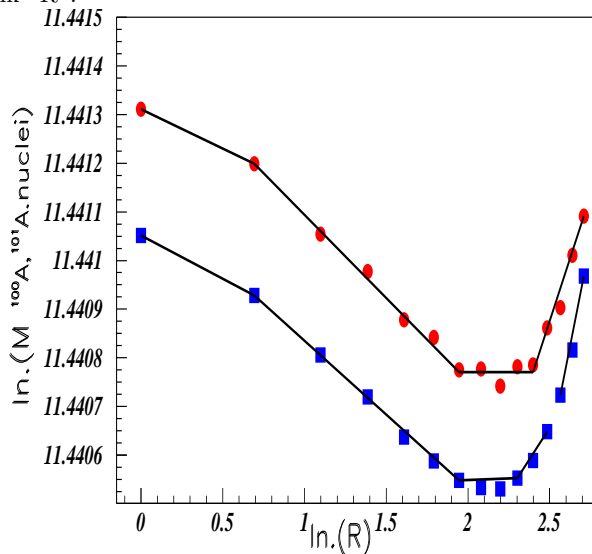
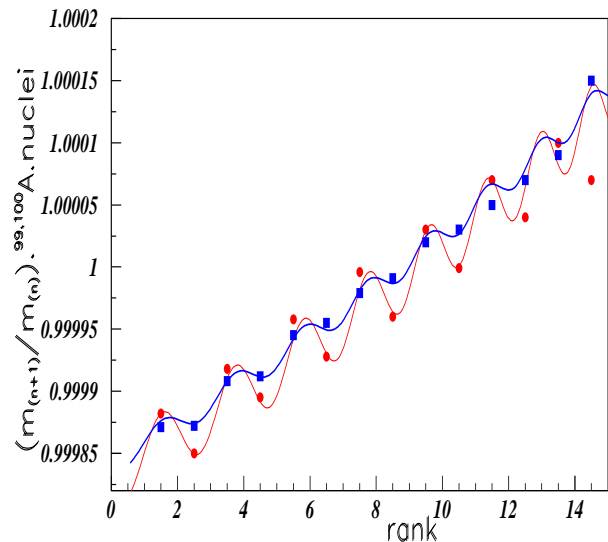


Figure 11 shows that many masses in the log-log plot of  $A = 100$  nuclei (full circles, red on line) and in the log-log

plot of  $A = 99$  nuclei (full squares, blue on line), can be described by a few straight lines. The  $A = 99$  distribution is shifted by 0.00978 in the y coordinate. These data should therefore follow the fractal properties. Here  $Z$  increases, for both distributions, from 36 (rank 1) up to 50 (rank 15). The  $m_{n+1}/m_n$  mass ratio of  $A = 100$  nuclei (full circles, red on line), are shown versus the rank  $R$  in figure 12. The  $m_{n+1}/m_n$  mass ratio of  $A = 99$  nuclei (full squares, blue on line), are shown versus the rank  $R$  in the same figure. They both exhibit many oscillations, very well fitted by equation (3) up to rank 15 (last rank). The oscillations are larger in case of even nucleus ( $A = 100$ ), than for odd nucleus ( $A = 99$ ). The ratio between both  $a_1$  factors, which describe the oscillation amplitude, is equal to 2.6.

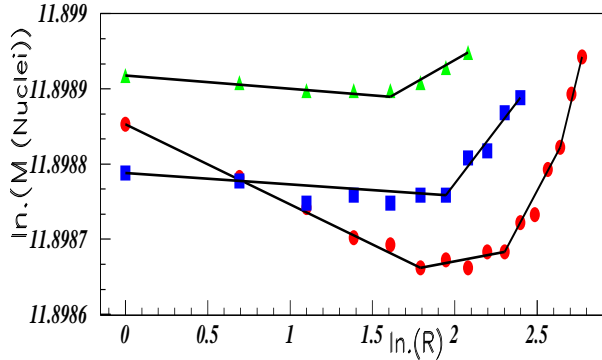
FIG. 12. Ratios of  $m_{n+1}/m_n$  masses versus the rank, for  $A = 100$  nuclei (full circles, red on line) and  $A = 99$  nuclei (full squares, blue on line).



### F. Application to some heavy nuclei with $A = 158$ , $192$ , and $251$

The next figure analyses the distributions for three heavier mass nuclei, in order to look at eventual fractal properties for intermediate and heavy mass nuclei. Figure 13 shows three log-log distributions for increasing  $Z$  values: full circles (red on line) show the distributions of  $A = 158$  nuclei,  $Z$  increasing from 59 (rank 1) up to 74 (rank 16); full squares (blue on line) show the distribution of  $A = 192$  nuclei, shifted by  $-0.195$ ,  $Z$  increasing from 74 (rank 1) up to 84 (rank 11); and full triangles (green on line) show the distribution of  $A = 251$  nuclei (green on line) shifted by  $-0.46353$  in y coordinate,  $Z$  increasing from 96 (rank 1) up to 103 (rank 8). These translations are done for clarity, in order to accept all three distribu-

FIG. 13. Log of some nuclei masses versus the log of the rank "R". Full circles (red on line), show the results for  $A = 158$  nuclei, full squares (blue on line), show the results for  $A = 192$  nuclei shifted by  $-0.195$ , and full triangles (green on line), show the results for  $A = 251$  nuclei shifted by  $-0.4633$ .



tions inside a same figure. We observe that distributions are well described by two straight lines for  $A = 251$  and  $192$ , and four straight lines for  $A = 158$  nuclei.

FIG. 14. Ratios of  $m_{n+1}/m_n$  masses for three different  $A$  values, versus the rank "R". Full circles (red on line), show the results for  $A = 158$  nuclei with increasing  $Z$  values, full squares (blue on line), show the distribution for  $A = 192$  nuclei, and full triangles (green on line), show the distribution for  $A = 251$  nuclei.

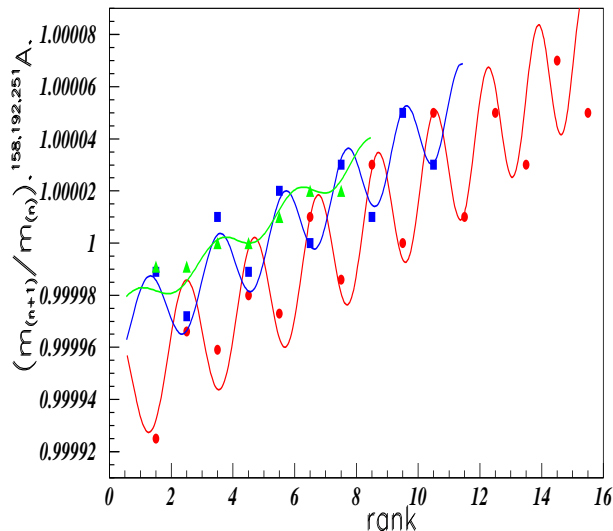


Figure 14 shows the ratios of  $m_{n+1}/m_n$  masses versus the rank "R", for the same three different  $A$  values, (and increasing  $Z$  values). Full circles (red on line), show the results for the  $A = 158$  nuclei, full squares (blue on line), show the distribution for  $A = 192$  nuclei, and full triangles (green on line), show the distribution for  $A = 251$  nuclei. The data exhibit oscillations which reduces when the masses increase. Here again, the experimental data are well fitted by equation (3).

## G. Application to masses of $A = 273$ nuclei

FIG. 15. Log of  $A = 273$  nuclei masses versus the log of rank "R".

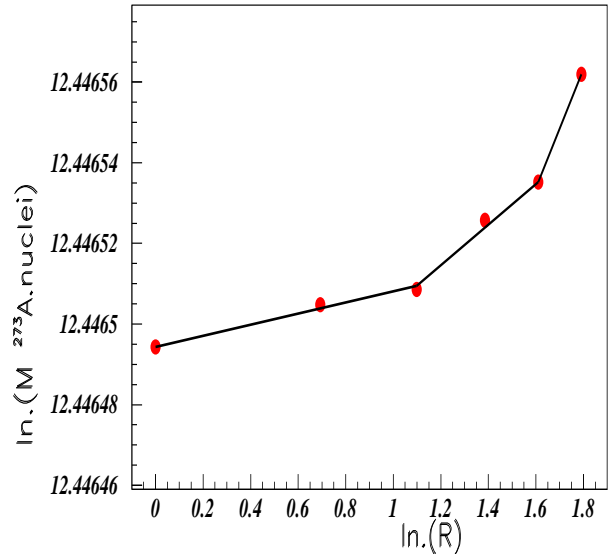
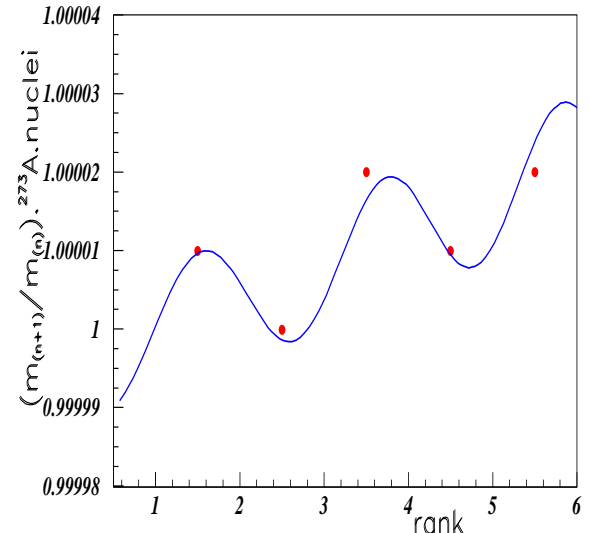


FIG. 16. Ratios of  $m_{n+1}/m_n$  masses versus the rank, for  $A = 273$  nuclei.



Only six masses of mass number  $A = 273$  nuclei are reported, and such small number does not allow a nice alignment of the log-log distribution shown in figure 15. The corresponding  $m_{n+1}/m_n$  mass ratio versus the rank, is shown in figure 16. As previously, the oscillations are well reproduced by the fit.

A precise prediction, concerning the eventual super-heavy and stable nuclei, is not possible. Indeed the

masses of unstable heavy nuclei, in the region where such superheavy nuclei are expected to exist, can be calculated using the mass excess table [11] and the alpha particle energies of the desexcitation chains. The energies of the  $\alpha$  particles of the desexcitation chains are known [12]; they differ one another by only a few MeV (close to 10 MeV). Starting from  $A=289$ ,  $Z=115$  nucleus, we could get heavier masses (adding two more  $\alpha$ ), but not nuclear masses with  $N = 184$ , and  $A = 298$ , or 304, or 310. In the same way, starting from  $A = 290$ ,  $Z = 115$  will not allow to get the masses indicated above.

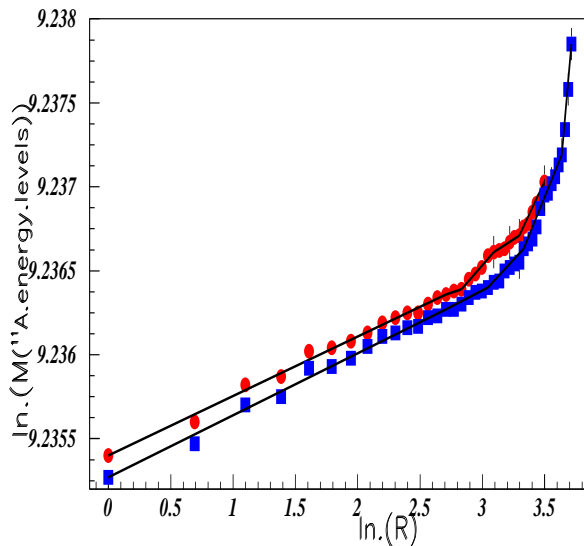
### III. APPLICATION TO EXCITED LEVEL NUCLEI MASSES

The excited level masses studied are introduced with increasing masses, starting from the fundamental one. The energy levels for different nuclei, are taken from several papers from F. Ajzenberg-Selove and T. Lauristen.

#### A. Application to excited level energies for nuclei masses $A=11,12$ , and 13

The excited level energies of  $A = 11$ , 12, and 13 nuclei, are taken from the Ajzenberg-Selove table [13].

FIG. 17. Log-log plot of excited level masses of  $^{11}\text{C}$  in full circles (red on line) and  $^{11}\text{B}$  in full squares (blue on line) .



We observe in figure 17, nice and parallel alignments of log-log distributions for the first 16 levels of  $^{11}\text{C}$  (full circles, red on line), and of  $^{11}\text{B}$  (full squares, blue on line). Figure 18 shows the corresponding  $m_{n+1}/m_n$  mass ratio distributions of  $^{11}\text{C}$  energy levels: full circles (red on line), and  $^{11}\text{B}$  energy levels: full squares (blue on line). The same set of parameters, allows, using equation (3),

FIG. 18. Ratios of  $m_{n+1}/m_n$  masses of  $^{11}\text{C}$  energy levels: full circles (red on line), and  $^{11}\text{B}$  energy levels: full squares (blue on line).

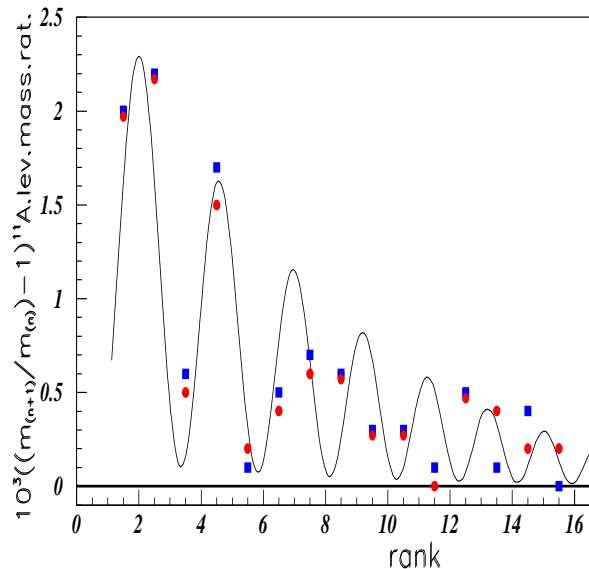
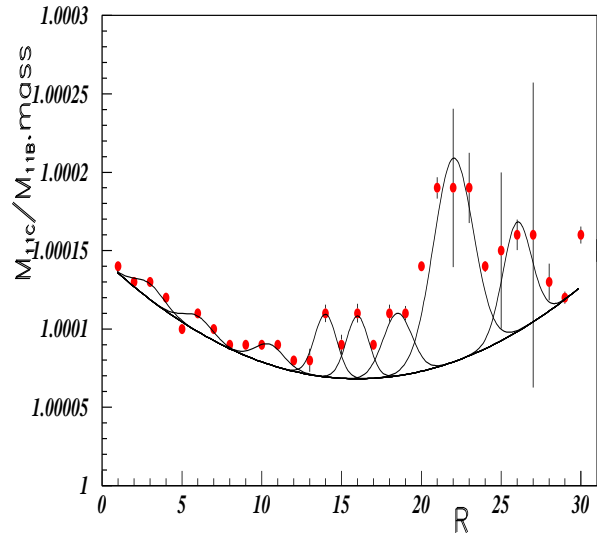


FIG. 19.  $^{11}\text{C}/^{11}\text{B}$  excited energy level ratios.

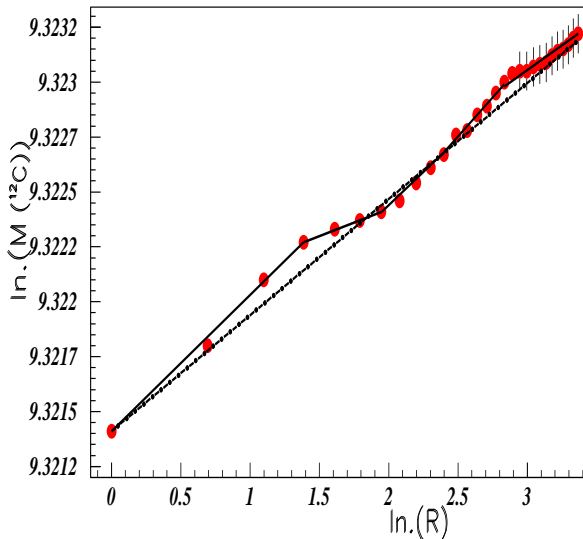
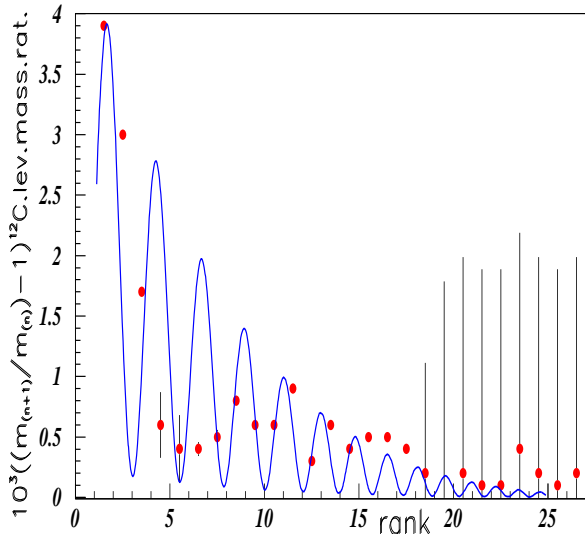


to well reproduce these ratios for both nuclei at least up to rank 11.

Figure 19 shows the  $^{11}\text{C}/^{11}\text{B}$  mass ratio, fitted by arbitrary gaussians in view to emphasize the oscillating behaviour of this ratio. Equation (3) does not allow to fit these data.

Figure 20 shows the log-log plot of the  $^{12}\text{C}$  excited energy level masses [13]. We observe a more or less nice alignment, with two slight shifts at the beginning (low "r"), and in the vicinity of the 17<sup>th</sup> level (mass = 17.76 MeV). Figure 21 shows the  $m_{n+1}/m_n$  mass ratios between adjacent  $^{12}\text{C}$  energy levels. Since the



FIG. 20. Log-log plot of energy level masses of  $^{12}\text{C}$ .FIG. 21. Ratios of  $m_{n+1}/m_n$  masses of  $^{12}\text{C}$  energy levels.

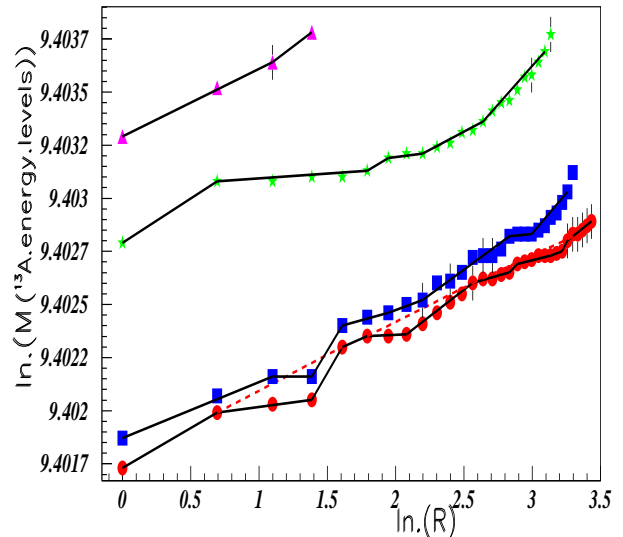
relative mass difference between adjacent levels is very small, a few MeV versus more than 11 GeV, The quantity  $1000 \cdot ((m_{n+1}/m_n) - 1)$  is plotted instead of  $m_{n+1}/m_n$ . When the mass precision is not given in the tables, an unprecision of 1 MeV is arbitrarily introduced for these uncertainties. The large error bars starting at  $R = 17.5$  manifest these large error arbitrarily introduced. The distribution fits all the fifteen first excited level masses, but the 2<sup>nd</sup>, 3<sup>rd</sup>, and 4<sup>th</sup> calculated maximas have no experimental counterpart. The ratio of rank 6.5 is far from the maximum of the calculated distribution at the same rank.

Figure 22 shows the log-log plot for  $A = 13$  excited level masses [13]. Full circles (red on line) show the plot for  $^{13}\text{C}$  nuclei, full squares (blue on line) show the plot for

$^{13}\text{N}$  nuclei, full stars (green on line) show the plot for  $^{13}\text{B}$  nuclei, and full triangles (purple on line) show the plot for  $^{13}\text{O}$  nuclei. The alignment of these lines, is not as good as it was for the  $^{11}\text{C}$  and  $^{11}\text{B}$  nuclei. The corresponding  $m_{n+1}/m_n$  mass ratios, shown in figure 23, are however well described by the DSI formula at least up to rank 16.

Figure 23 shows the  $m_{n+1}/m_n$  mass ratios of excited

FIG. 22. Log-log distribution of  $A = 13$  excited level masses. Full circles (red on line) show the plot for  $^{13}\text{C}$  nuclei, full squares (blue on line) show the plot for  $^{13}\text{N}$  nuclei, full stars (green on line) show the plot for  $^{13}\text{B}$  nuclei, and full triangles (purple on line) show the plot for  $^{13}\text{O}$  nuclei.



levels for  $A = 13$  nuclei. The curve corresponds to a fit obtained using equation (3). As before, we observe a unique and rather good fit for all four  $A = 13$  nuclei, up to  $R = 16$ , which spoils for larger  $R$  values.

### B. Application to $^{14}\text{C}$ energy levels

Figure 24 shows the log-log plot of  $^{14}\text{C}$  energy level masses [14]; several straight lines are observed.

Figure 25 shows the  $m_{n+1}/m_n$  mass ratios of  $^{14}\text{C}$  levels. We observe here a case where the equation (3) does not allow to fit the experimental data. Two fits are drawn, both describe well the "peak" around rank 8. The first fit (black on line), catches also the first large point, but forgets both the data after rank 11 and the data for rank 2 and 3. The second fit (blue on line) forgets completely the first four data points. None are satisfactory.

### C. Application to $^{16}\text{O}$ energy levels

Figure 26 shows the log-log plot for  $^{16}\text{O}$  nuclei level masses [15]. A large number of nuclear level masses are given in the table, but their definition spoils for

FIG. 23. Ratios of  $m_{n+1}/m_n$  masses of excited levels of  $A = 13$  nuclei. Full circles (red on line) show the distribution for  $^{13}\text{C}$  nuclei, full squares (blue on line) show the distribution for  $^{13}\text{N}$  nuclei, full stars (green on line) show the distribution for  $^{13}\text{B}$  nuclei, and full triangles (purple on line) show the distribution for  $^{13}\text{O}$  nuclei.

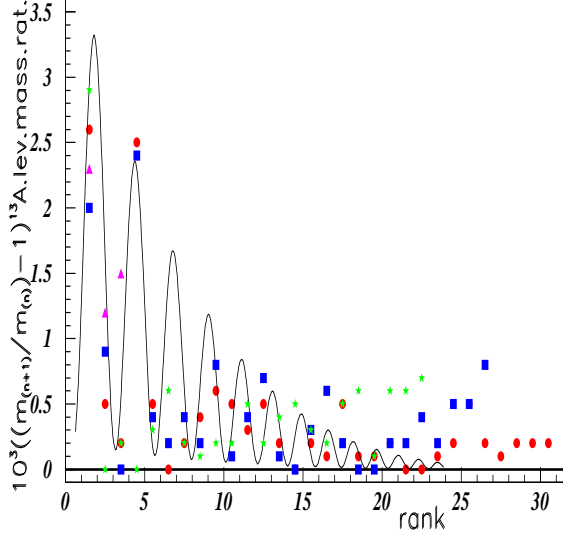
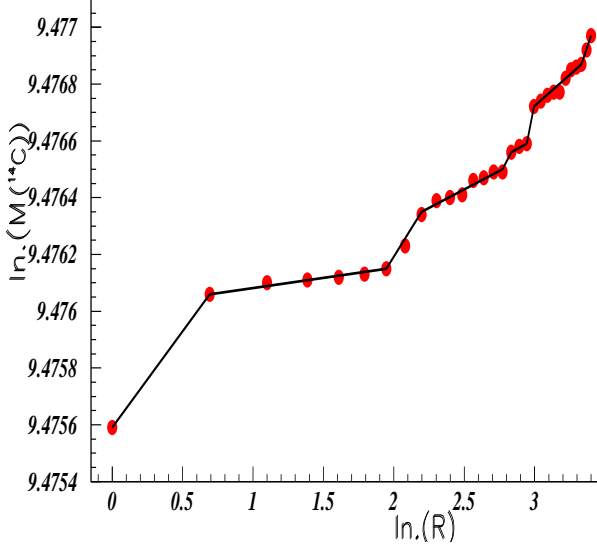


FIG. 24. Log-log plot of energy level of  $^{14}\text{C}$ .



energy levels with an excitation energy larger than  $\Delta M=13$  MeV (see insert (a)). Therefore a reduced number of log-log distributions of level masses is represented in figure 26(b). A nice alignment is disturbed between 6 and 7 MeV excitation energy, and in the region close to 9 - 10 MeV excitation energy. Figure 27 shows the  $m_{n+1}/m_n$  excited level mass ratios of  $^{16}\text{O}$  levels. The data points are reasonably fitted by equation (3) up to  $R=14.5$ , but with different parameters as those used for  $A = 11, 12$ , and  $13$  shown in previous figures. In the

FIG. 25. Ratios of  $m_{n+1}/m_n$  masses of  $^{14}\text{C}$ .

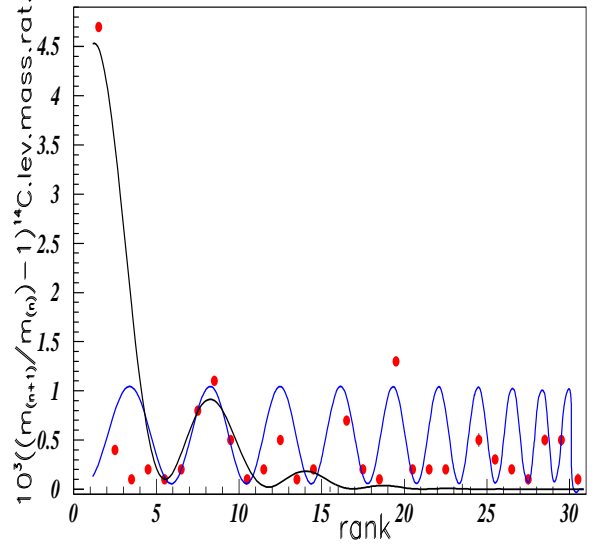


FIG. 26. Log-log plot of energy level masses of  $^{16}\text{O}$  nucleus (see text).

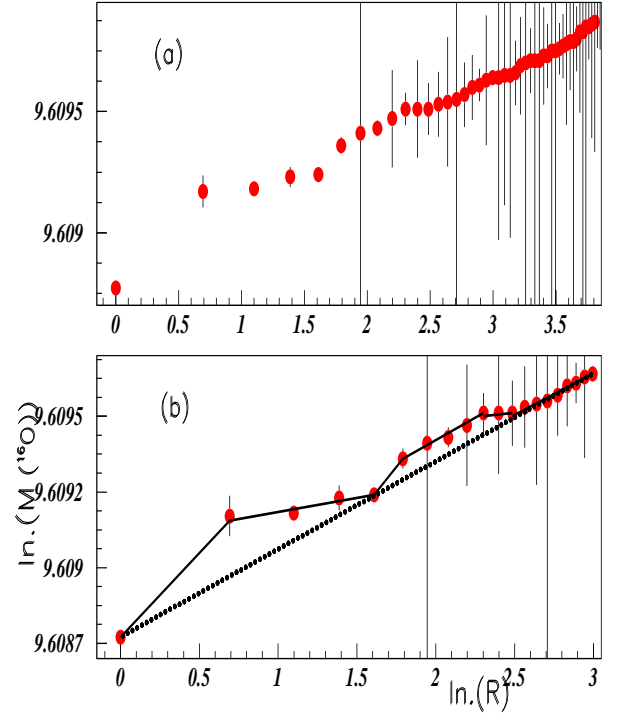
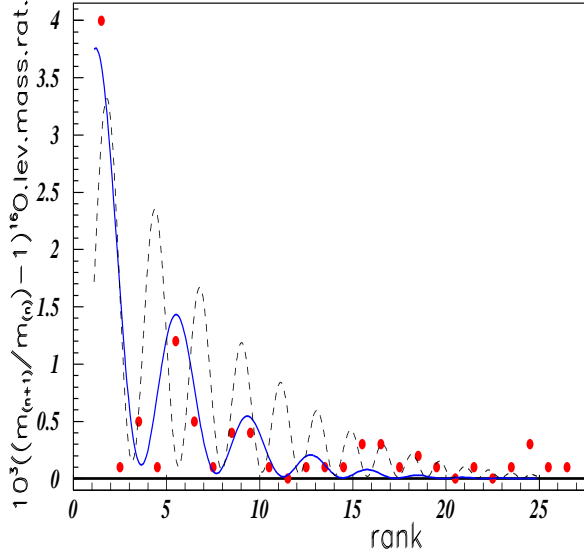
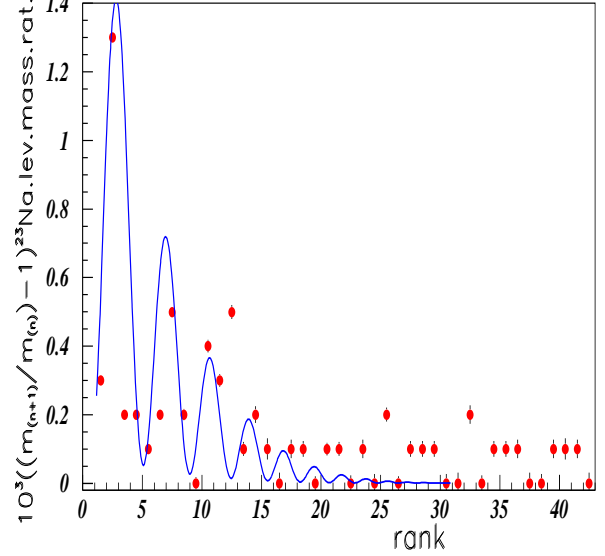
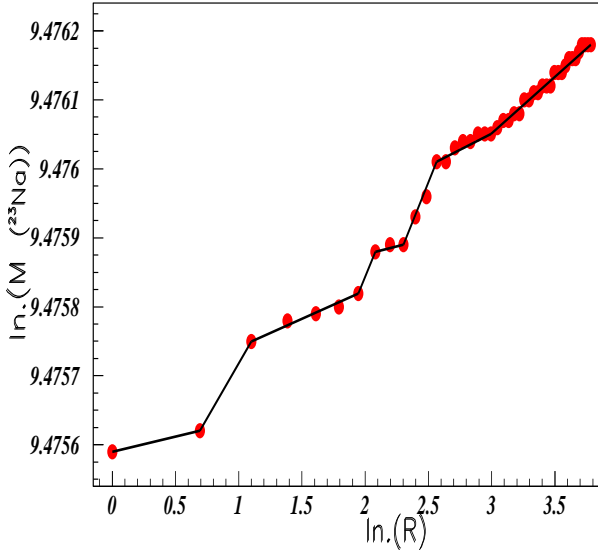


figure 27, the dashed curve shows the fit obtained when the parameters fitting the  $C = 13$  nuclei, are used.

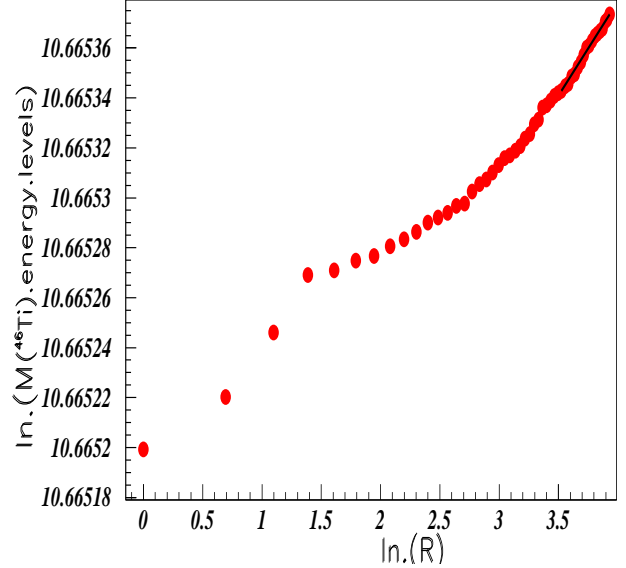
FIG. 27. Ratios of  $m_{n+1}/m_n$  excited level masses of  $^{16}\text{O}$ .FIG. 29. Ratios of  $m_{n+1}/m_n$  masses of  $^{23}\text{Na}$  energy levels.FIG. 28. Log-log plot of  $^{23}\text{Na}$  energy level masses.

#### D. Application to $^{23}\text{Na}$ nucleus

Figure 28 shows the log-log distribution of the energy levels of the  $^{23}\text{Na}$  nucleus [16]. It exhibits several, too short straight lines. The corresponding  $m_{n+1}/m_n$  excited level mass ratio distributions, shown in figure 29, display an oscillatory pattern, rather well described by equation (3) up to rank 11.

#### E. Application to $^{46}\text{Ti}$ nucleus

Figure 30 shows the log-log distribution of the energy levels of the  $^{46}\text{Ti}$  nucleus [17]. The linearity between the

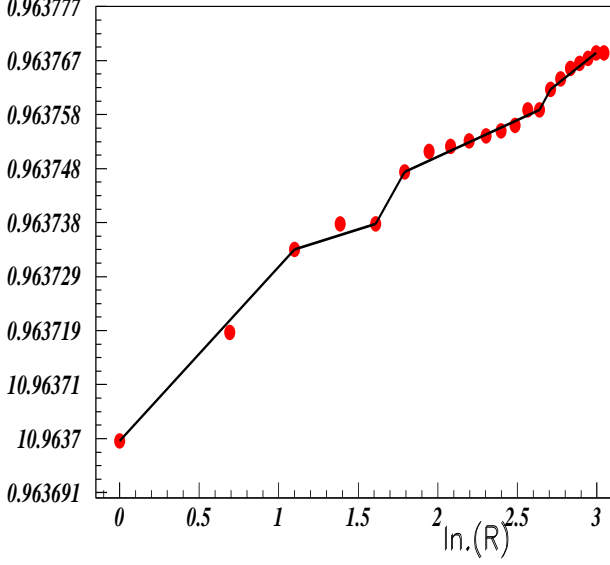
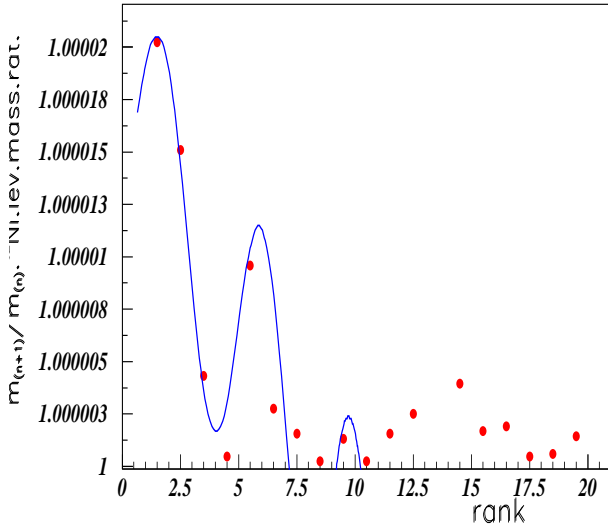
FIG. 30. Log-log plot of energy levels of  $^{46}\text{Ti}$ .

log of the masses versus the log of the rank, is not really observed, at least for the first 14 masses. Therefore the corresponding  $m_{n+1}/m_n$  mass ratio is not studied.

#### F. Application to $^{62}\text{Ni}$ nucleus

Figure 31 shows the log-log distribution of the energy levels of the  $^{62}\text{Ni}$  nucleus [18]. The distribution exhibits several, straight lines, except the fourth excited level mass,  $M = 2.336$  MeV, which is outside the linearity.

The corresponding  $m_{n+1}/m_n$  excited level mass ratio distribution, shown in figure 32 displays an oscillatory pattern, well described by equation (3) up to rank 11.

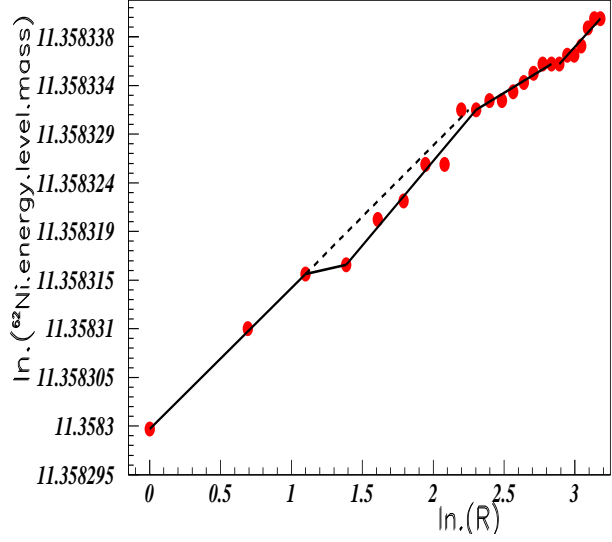
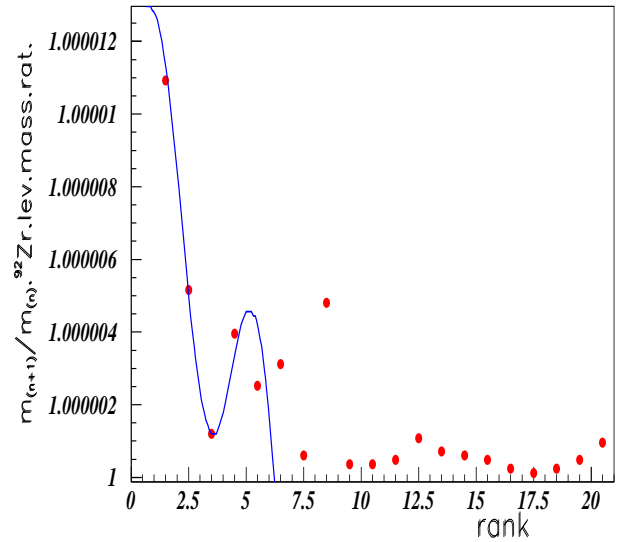
FIG. 31. Log-log plot of energy level of  $^{62}\text{Ni}$ .FIG. 32. Ratios of  $m_{n+1}/m_n$  masses of  $^{62}\text{Ni}$ .

Here also, the very close to one value of the ratio between two adjacent masses, leads us to keep only the first term of the limited development of the  $\ln(1+x)$  function.

### G. Application to $^{92}\text{Zr}$ excited level masses

Figure 33 shows the log-log distribution of the energy levels of the  $^{92}\text{Zr}$  nucleus [19]. The distribution exhibits some straight lines.

The corresponding  $m_{n+1}/m_n$  mass ratio distribution, shown in figure 34, displays an oscillatory pattern, well described by equation (3) but only up to rank 6, in a much smaller range than before. Here also, the very close to one value of the ratio between two adjacent masses, leads to keep only the first term of the limited devel-

FIG. 33. Log-log plot of  $^{92}\text{Zr}$  of energy level masses.FIG. 34. Ratios of  $m_{n+1}/m_n$  masses of  $^{92}\text{Zr}$ .

opment of the  $\ln(1+x)$  function.

### H. Application to $^{134}\text{Ba}$ the energy level masses

Figure 35 shows the log-log distribution corresponding to  $^{134}\text{Ba}$  nucleus energy level masses [20]. A long straight line is observed for this nuclei; a nice fit is also observed, up to rank  $R = 8$ , for the  $^{134}\text{Ba}$   $m_{n+1}/m_n$  mass ratio versus the rank "R", shown in figure 36.

## IV. DISCUSSION

The values extracted from the fits analysing the mass ratios, are given in table 1. Although, it is not possible to

FIG. 35. Log of the energy level masses of the  $^{134}\text{Ba}$  nucleus versus the log of the rank "R"

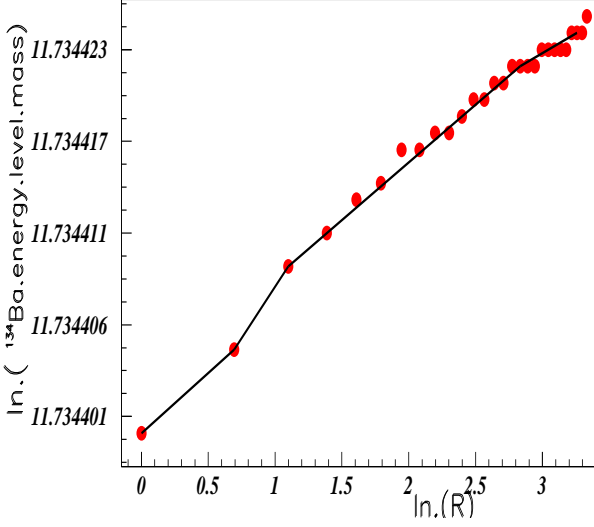
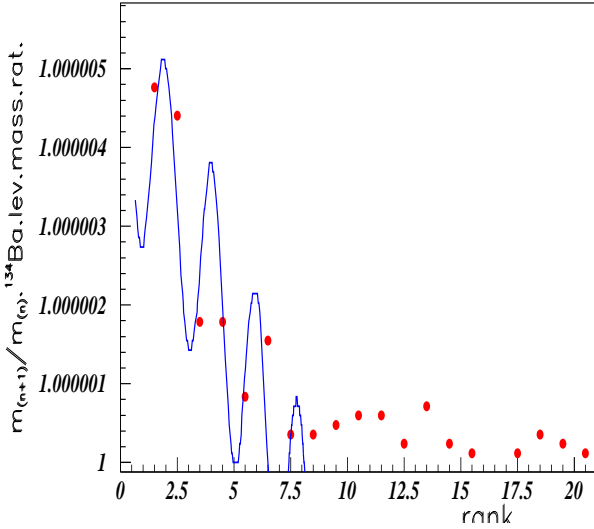


FIG. 36. Ratios of  $m_{n+1}/m_n$  masses for  $^{134}\text{Ba}$  nucleus

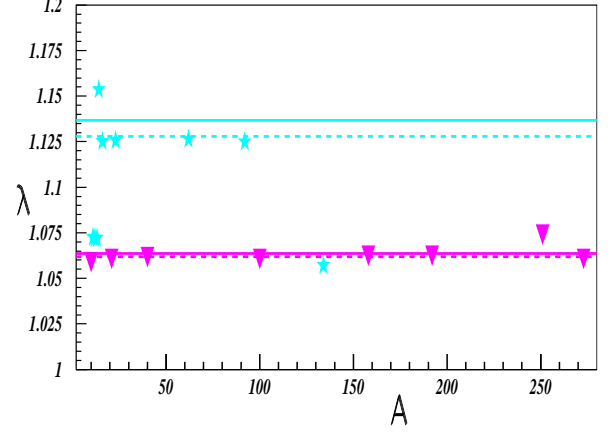


give the precisions on these parameters, we observe that an unique curve, describing the data, is plotted in figures 18 and 23, although the parameters shown in table III, differ a little. This gives an idea of the parameter uncertainty. The data differ from fit, always beyond  $R = 16$ , sometimes before.

The parameters, obtained from section II, studying the nuclei mass variations, describe the complete distributions and are therefore stronger than those determined from excited level energies (section III), for which only the beginning of the distributions are well fitted. We observe that the range of linearity in the log-log distribution, does not always correspond to the range of nice fit, between the mass ratio data and the curve obtained using equation (3).

Considering the parameters obtained from nuclei

FIG. 37. Variation of  $\lambda$  values versus  $A$ . Full triangles (mauve on line) show the values extracted from nuclei mass variations. Full stars (sky blue on line) show the values from nuclei energy level masses.



masses, we observe:

- all  $\Omega$  values are close, except that from  $A = 251$  which is a little lower: 14 instead of 17. Therefore the  $\lambda$  and  $\text{Im}(\alpha)$  are also almost constant,
- $a_1$  and  $\text{Re}(\alpha)$  decrease for increasing masses  $A$ .
- all  $\mu$  are equal or close to 1.

Considering the parameters obtained from nuclei excited levels, we observe:

- two distinct  $\Omega$ , therefore  $\lambda$  and  $\text{Im}(\alpha)$  values, have been extracted. The first one, close to 14.2, is again a little lower than  $\Omega = 17$ , observed in the nuclei masses studies (except for  $^{134}\text{Ba}$ , figure 36). The second value is  $\Omega \approx 8.2$ . The transition occurs between masses  $A = 13$  and  $A = 14$ ,
- the  $a_1$  parameters are much larger than before, except for the two heavier nuclei studied:  $^{92}\text{Zr}$  and  $^{134}\text{Ba}$ , where it takes the same value as previously in heavy nuclei mass fits, namely  $a_1 \leq 10^{-4}$ .
- $\mu$  equals 1 three times, equals 1.4 seven times, equals 2 two times, and equals 2.6 one time. These number are respectively close to the square roots of 1, 2, 4, and 7. The variation of  $\mu$  is due to two opposite effects: an increase for stable nuclei close to magic numbers, in comparison with less stable nuclei, and a decrease for larger mass nuclei, since it is the relative mass variation which is concerned. This second effect is the main one for heavy nuclei, as seen in table 1 for  $^{92}\text{Zr}$  and  $^{134}\text{Ba}$  nuclei.

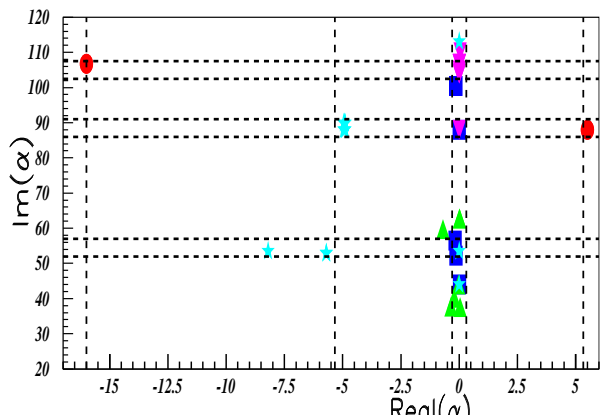
Figure 37 shows the values of the fundamental scaling ratio  $\lambda$  versus  $A$ . In figure 37, full triangles (mauve on line) show the values extracted from nuclei mass variations. These values are constant around  $\lambda_1 = 1.062$  (dashed straight line, mauve on line) with a very small variation around this mean value. Since several fits give the same values for  $\lambda$ , the figure shows less points than obtained by fits.

Full stars (sky blue on line) show the values from the

nuclei excited energy level masses. Four of them, extracted from light and heavy nuclei, have the same  $\lambda$  value, namely  $\lambda_2 \approx 1.128$ , shown in figure 37 by a dashed straight line (sky blue on line). Two other  $\lambda$  values are close to 1.062. Such property was anticipated in [7] where it was noticed that "DSI obeys scale invariance for specific choices of  $\lambda$ , which form an infinite set of values that can be written as  $\lambda_n = \lambda^n$ . Indeed here  $\lambda_2 = \lambda_1^2$ .

Notice that the low  $\lambda$  value is close to the  $\lambda$  observed previously [6] for quarks:  $\lambda = 1.074$  and leptons:  $\lambda = 1.061$ . Just as closed  $\lambda$  values were extracted from the fits which analyzed in the same way the fractal properties of mesons and baryons [9]. Then regrouping all  $\lambda$  values obtained through fits performed on quarks, leptons, hadrons and nuclei, we get the two continuous lines drawn in figure 37, where we have shared the  $\lambda$  into two groups. The first group leads to the first mean value  $\bar{\lambda}_1 = 1.064$ , using all  $\lambda \leq 1.1$ ; the second group use  $\lambda \geq 1.1$  giving  $\bar{\lambda}_2 = 1.137$ . We notice that we still have  $\bar{\lambda}_2 = \bar{\lambda}_1^2$ .

FIG. 38. Plot of  $\text{Im}(\alpha)$  versus  $\text{Re}(\alpha)$ . Full circles (red on line) show the  $\alpha$  values which fit the elementary particle quark and lepton mass distributions; full up side triangles (green on line) show the same for meson data; full squares (blue on line) show the same for baryon data; full down side triangles (purple on line) show the same for nuclei mass variation data; and full stars (blue sky on line) show the same for nuclei energy level mass data.



In order to draw the last figure (figure 38), we not only use the  $\alpha$  values obtained from the fits performed above through the study of the nuclei masses and nuclei energy levels. We also use the  $\alpha$  values obtained in a previous work [6] studying the quark mass ratios, and also the  $\alpha$  values obtained in a previous work [9] studying the hadron properties applied to hadron (meson and baryon) spectroscopies. These parameters are given in table IV.

Figure 38 shows the  $\text{Im}(\alpha)$  versus  $\text{Re}(\alpha)$  plot. Full circles (red on line) show the  $\alpha$  values which fit the elementary particle quark and lepton data; there values differ strongly from the others.

Full up side triangles (green on line) show the same for meson data; the corresponding  $\text{Re}(\alpha)$  is stable, close to zero, when the imaginary part varies from 37 up to 63.

Full squares (blue on line) show the same for baryon data; the real part of  $\alpha$  is stable close to zero, when the imaginary part moves from 44 up to 101.

Full down side triangles (purple on line) show the same for nuclei mass variation data; here  $\text{Re}(\alpha) \approx 0$  is again stable and the imaginary part varies a little around  $104 = 2 * \pi / \ln(\bar{\lambda}_1)$ .

Full stars (blue sky on line) show the same for nuclei energy level mass data. A great number of marks (seven) are not apparent, since they have the same value:  $\alpha = -4.9 + 89 * i$ . The other six marks scatter. All in all, we have once  $\text{Re}(\alpha) \approx -16$ , once  $\text{Re}(\alpha) \approx -8.2$ , 3 times  $\text{Re}(\alpha) \approx 23$ , 3 times  $\text{Re}(\alpha) \approx 0$ , and 7 times  $\text{Re}(\alpha) \approx 5.3$ .

The marks therefore are not distributed randomly; this is emphasized by dashed lines. There are two distinct  $\text{Im}(\alpha)$  values for excited nuclei energy level masses. These two values correspond to the two distinct values of  $\lambda$ . At the same values, we observe  $\text{Im}(\alpha)$  for mesons, quarks, leptons, and data from nuclei mass variation data. All data, except quark, lepton, and data from nuclei energy level masses have  $\text{Re}(\alpha) \approx 0$ .

In addition to the  $\mu$  values, obtained from fits performed on fractal properties on nuclei, the  $\mu$  values from elementary particle fits, and hadron fits, reported in table IV, introduce only four new values. They are  $\mu = 0.675$  (from quark distribution), 1.08 (unflavored mesons), 1.035 (charmed mesons), and 1.018 ( $\Sigma$  and  $\Xi$  baryons.)

In summary, the analysis of fractal properties of elementary particles masses, hadronic masses, and nuclei masses and energy levels, lead to a rather small number of parameters, much smaller than the very large number of data analysed here (several hundreds).

## V. CONCLUSION

We have shown that nuclear physics masses and nuclei energy level masses, as well as elementary particle masses, have often fractal properties and that they verify the discrete-scale invariance properties. Indeed the imaginary part of  $\alpha$  is usually more than 18 times larger than the corresponding real part. We are therefore far from continuous scale invariance. In this model, "the system of the observables obeys scale invariance for specific choices of  $\lambda$  (and therefore  $\mu$ )" [7].

The fractal property of log-log straight line between the masses of several nuclei and their ranks was used to predict some masses of still unobserved nuclei.

The equation used to describe the relative mass increase - equation (3) - allows to reproduce accurately the total spectra of mass variations studied in section II. On the other hand, the fits corresponding to the study of the excited energy levels (section III), reproduce only a part of the used data. Moreover only about 20 data are considered, whereas a much larger number is known. The agreement of theory and data is therefore weaker concerning this part of the analysis.

The analysis of the fractal properties of elementary particles masses, hadronic masses, and nuclei masses and energy levels, leads to a reduced number of parameters, when compared to the large number of masses concerned, masses which therefore appear to be correlated.

## VI. ACKNOWLEDGMENTS

Felix Scholkmann is acknowledged for having pointed out to my attention, the papers studying the particle

masses within the Model of Oscillations in a Chain System [3].

- 
- [1] B. Mandelbrot, *Les objets fractals* (Flammarion, Paris 1975), *ibid The Fractal geometry of Nature* (Freeman, San Francisco, 1982).
  - [2] J. Chaline, L.Nottale, and P. Grou, avec la participation d'Ivan Brissaud; "Des Fleurs pour Schrödinger, la Relativité d'échelle et ses applications", ed. Ellipses Éditions, 2009.
  - [3] H. Müller, *Progress in Physics*, **3**, 61 (2010); A. Ries and M. V. Lia Fook, *Progress in Physics*, **4**,82 (2010).
  - [4] E. Goldfain, *Prespacetime Journal* **2**, 523 (2011).
  - [5] B. Tatischeff and I. Brissaud, arXiv:1005.0238v1 [hep-ph] (2010).
  - [6] B. Tatischeff arXiv:1104:5379v1 [physics.gen-ph] (2011).
  - [7] D. Sornette, *Physics Reports* **297**, 239 (1998).
  - [8] L. Nottale, The Theory of Scale Relativity: Non-Differentiable Geometry and Fractal Space-Time. In : Computing Anticipatory Systems. CASY'S03 - Sixth international Conference (Liège 2003), D.M. Dubois, Ed., American Institute of Physics Conference proceedings, 718, p.68 (2004).
  - [9] B. Tatischeff arXiv:1105:2034 v1 [physics.gen-ph] (2011).
  - [10] The subsections A and B reproduce the model description presented in [9]. They are repeated here for a complete description.
  - [11] G. Audi, A.H. Wapstra, and C. Thibault, *Nucl. Phys.* **A729**, 337 (2003).
  - [12] Yu.Ts. Oganessian *et al.*, *Phys. Rev. Lett.* **104**, 142502-1 (2010).
  - [13] F. Ajzenberg-Selove and T. Lauristen, *Nucl. Physics A*(**506**, 1 (1990), *ibid*Nucl. Physics **A523**, 1 (1991).
  - [14] F. Ajzenberg-Selove and T. Lauristen, *Nucl. Physics A***523**, 1 (1991); F. Ajzenberg-Selove , H.G. Bingham, and J.D. Garrett, *Nucl. Phys.* **A202**, 152 (1973).
  - [15] F. Ajzenberg-Selove and T. Lauristen, *Nucl. Physics A***460**, 1 (1986).
  - [16] J. Dubois, *Nucl. Phys.* **A99**, 465 (1967).
  - [17] L. Broman and D.J. Pullen, *Nucl. Phys.* **A110**, 161 (19678).
  - [18] D.L. Kennedy, H.H. Bolotin, I. Morrison, and K. Amos, *Nucl. Phys.* **A308**, 14 (1978).
  - [19] T. Borello-Lewin, H.M.A. Castro, L.B. Horodyski-Matsushigue, and O. Dietzsch, *Phys. Rev. C***20**, 2101 (1979).
  - [20] *Physics 77*, table of isotopes, Firestone and Shirley, Editors.

TABLE III. Parameters of the nuclear mass ratio and nuclear energy level fits.

sect.	fig.	nuclei	$\Omega$	$a_1$	$\lambda$	$\text{Re}(\alpha)$	$\text{Im}(\alpha)$	$\mu$
nucl.	5	A=10	17.5	$7.0 \cdot 10^{-4}$	1.059	$3.8 \cdot 10^{-2}$	110.0	.998
mass	7	21	17	$2.6 \cdot 10^{-4}$	1.061	$1.2 \cdot 10^{-2}$	106.8	.999
	9	40	16.7	$1.2 \cdot 10^{-4}$	1.062	$4.0 \cdot 10^{-3}$	104.9	1.
II		42	16.7	$1.2 \cdot 10^{-4}$	1.062	$4.0 \cdot 10^{-3}$	104.9	1.
		38	16.7	$1.2 \cdot 10^{-4}$	1.062	$4.0 \cdot 10^{-3}$	104.9	1.
	12	99	17.0	$1.0 \cdot 10^{-5}$	1.061	$6.4 \cdot 10^{-4}$	106.8	1.
		100	17.0	$2.6 \cdot 10^{-5}$	1.061	$6.4 \cdot 10^{-4}$	106.8	1.
	14	158	16.5	$2.5 \cdot 10^{-5}$	1.062	$2.7 \cdot 10^{-4}$	104.0	1.
		192	16.5	$1.5 \cdot 10^{-5}$	1.062	$2.7 \cdot 10^{-4}$	104.0	1.
		251	14.0	$5.0 \cdot 10^{-6}$	1.074	$2.7 \cdot 10^{-4}$	88.0	1.
	16	273	17.0	$8.0 \cdot 10^{-6}$	1.061	$1.6 \cdot 10^{-4}$	106.8	1.
nucl.	18	$^{11}\text{C}$	14.3	0.9	1.072	-4.9	89.8	1.4
exci.		$^{11}\text{B}$	14.0	.62	1.074	-4.9	88.0	1.42
ener.	21	$^{12}\text{C}$	14.3	0.9	1.072	-4.9	89.9	1.4
level	23	$^{13}\text{C}$	14.3	0.9	1.072	-4.9	89.9	1.4
III		$^{13}\text{N}$	14.0	.62	1.074	-4.95	88.0	1.42
		$^{13}\text{B}$	14.3	1.0	1.072	-4.95	89.8	1.41
		$^{13}\text{O}$	14.0	.62	1.074	-4.9	88.0	1.42
	25	$^{14}\text{C}$	7	0.9	1.154	0	44.0	1.
	27	$^{16}\text{O}$	8.5	0.9	1.125	-8.2	53.4	2.62
	29	$^{23}\text{Na}$	8.45	0.9	1.126	-5.7	53.0	1.96
	32	$^{62}\text{Ni}$	8.4	0.9	1.126	-5.7	52.8	1.97
	34	$^{92}\text{Zr}$	8.5	$3.5 \cdot 10^{-6}$	1.125	$-7 \cdot 10^{-5}$	53.4	1.
	36	$^{134}\text{Ba}$	18.0	$1.5 \cdot 10^{-6}$	1.057	$-2.6 \cdot 10^{-5}$	113	1.

TABLE IV. Parameters of the quark, lepton, and hadronic mass fits. The data corresponding to quark and lepton fits, have been published in [6]; the data corresponding to hadronic mass fits, have been published in [9].

part.	fig.	nuclei	$\Omega$	$a_1$	$\lambda$	$\text{Re}(\alpha)$	$\text{Im}(\alpha)$	$\mu$
quark	5	quark	14	1	1.074	5.5	88	.675
lept.	5	leptons	17	1.2	1.061	-16	106.8	2.56
meson	3	unflavo.	9.5	0.11	1.111	-0.7	59.7	1.08
			7	.014	1.154	-.02	44	1.00
	5	strange	10	.018	1.105	.015	62.8	.998
	7	charmed	6.4	0.03	1.169	-.22	40.2	1.035
	9	cha.str.	6	.021	1.181	-.35	37.7	1.06
	13	$c - \bar{c}$	10	.018	1.105	.015	62.8	.998
	15	$b - \bar{b}$	5.99	.008	1.182	0.04	37.6	.993
baryon	17	N	14	0.04	1.074	0	88	1
	20	$\Lambda$	7	0.04	1.154	0.01	44	.999
	22	$\Sigma$	8.3	.014	1.128	-.14	52.2	1.017
	24	$\Xi$	9	.022	1.118	-.17	56.5	1.019
	26	charmed	16	.022	1.064	-.15	100.5	1.01
	28	$\Xi_c$	16	.018	1.064	-.15	100.5	1.01